Experimental and numerical study on the thermal behavior of phase change material infiltrated in low porosity metal foam

Xusheng Hu, Feng Zhu, Xiao-Lu Gong

▶ **To cite this version:**

Xusheng Hu, Feng Zhu, Xiao-Lu Gong. Experimental and numerical study on the thermal behavior of phase change material infiltrated in low porosity metal foam. Journal of Energy Storage, 2019, 26, pp.101005. 10.1016/j.est.2019.101005 . hal-02366379v2

HAL Id: hal-02366379
https://utt.hal.science/hal-02366379v2

Submitted on 21 Dec 2021

HAL is a multi-disciplinary open access archive for the deposit and dissemination of scientific research documents, whether they are published or not. The documents may come from teaching and research institutions in France or abroad, or from public or private research centers.

L'archive ouverte pluridisciplinaire **HAL**, est destinée au dépôt et à la diffusion de documents scientifiques de niveau recherche, publiés ou non, émanant des établissements d'enseignement et de recherche français ou étrangers, des laboratoires publics ou privés.

Distributed under a Creative Commons Attribution - NonCommercial 4.0 International License

Version of Record: https://www.sciencedirect.com/science/article/pii/S2352152X19306656
Manuscript_82e30b406bd61f7e7b47bfbe888b6993

Experimental and numerical study on the thermal behavior of phase change material infiltrated in low porosity metal foam

Xusheng Hu[a], Feng Zhu[a,b], Xiaolu Gong[a,*]
[a]Charles Delaunay Institute, LASMIS, University of Technology of Troyes, 12 Rue Marie Curie, 10004 Troyes, France
[b]Institute of electrical engineering, Chinese academy of sciences, Beijing 100190, China
(*) Correspondent author, gong@utt.fr

Abstract

In this paper, a comprehensive experimental and numerical investigation is conducted to study the thermal behavior of phase change material (PCM) infiltrated in low porosity metal foam (LPMF). A visible experiment is designed to trace the temperature field and solid-liquid melting evolvement of PCM with and without metal foam. The experimental method and pore-scale numerical simulation are employed to extract temperature histories at different location during the melting process. Besides, the effective thermal conductivity of composite PCM is calculated by numerical simulation and compared with the theoretical models. Experimental results indicate that the thermal behavior of PCM can be visibly enhanced by embedding LPMF, e.g., by comparing with pure paraffin, the melting time of composite PCM is reduced by 45% and the maximum temperature difference is decreased by 83.3%. The porosity has influences on the thermal characteristics of composite PCMs. Numerical results exhibit good agreement with experimental data, which indicates that modified Kelvin model can be employed to predict the thermal performance of composite PCM. Also it can be found from numerical results that effective thermal conductivities of composite PCMs are distinctly heightened, e.g., the effective thermal conductivities of composite PCM with 67% porosity is about 108 times as much as that of paraffin. Numerical model is of great significance for study and design of thermal management system using composite PCM.

Keywords: Phase change material, Low porosity metal foam, Numerical simulation, Modified Kelvin model, Thermal behavior

© 2019 published by Elsevier. This manuscript is made available under the CC BY NC user license
https://creativecommons.org/licenses/by-nc/4.0/

Nomenclature			
A_m	mush constant	t	time (s)
C	specific heat capacity (J/kg · K)	V	volume (m^3)
c	smaller constant	u	velocity (m/s)
f_l	liquid fraction		
G_r	Grashof number	Greek symbols	
g	gravitational acceleration (m/s^2)	ε	porosity
h	heat transfer coefficient ($W/m^2 \cdot K$)	γ	thermal expansion coefficient (1/K)
k	thermal conductivity (W/m · K)	μ	dynamic viscosity (kg/m · s)
L	latent heat (J/kg · K)	ρ	density (kg/m^3)
m	mass (kg)		
P_r	Prandtl number	Subscripts	
p	pressure (Pa)	*eff*	effective value
S	source term	p	paraffin
T	temperature (K)	f	aluminum foam

1. Introduction

In recent years, the global energy crisis is increasingly severe. The renewable energy resource and energy saving technology attract extensive attention, such as solar energy [1], energy efficient building [2], electric vehicles [3], etc. Thermal management system (TMS) plays an important role in the new energy utilization [4]. Phase change material is widely applied in passive or hybrid passive thermal management system owing to the high latent heat and steady phase change temperature during the energy storage [5, 6]. However, the disadvantage of PCM is the lower thermal conductivity, which reduces heat transfer rate and hinders its application in TES [7]. Many methods are developed to heighten its thermal behavior, such as inserting metal fins and pins [8, 9], encapsulated PCMs [10, 11], adding high thermal conductivity additive [12, 13] and embedding metal foam [14-16]. It is proved that the embedding metal foam is an effective approach for the improvement of thermal performance of PCM.

The high porosity metal foam (HPMF) is usually made by the electro-deposition method and investment casting method, which possesses high porosity (the porosity ranges from 80% to 99%) and permeability [17]. Bhattacharya et al. [18] performed a study on thermophysical properties of HPMF by using the analytical and experimental approach. Lafdi et al. [19] designed an experiment to study the influences of porosity and pore size on the melting evolvement of PCM saturated in aluminum foam with porosities ranging from 88.4% to 96%. Yang et al [20, 21]. carried out the experimental and numerical investigation for influences of PCM saturated in metal foam on the thermal energy storage unit, and they demonstrated that embedding metal foam can distinctly strengthen heat transfer and improve temperature uniformity. Xiao et al. [26] prepared composite PCM which is made of metal foam and paraffin adopting the vacuum impregnation method and performed an experimental test on the thermal characterization of composite PCM with porosities larger than 95%.

The low porosity metal foam (LPMF) can be manufactured by the infiltration casting method. Its porosity is lower and usually ranges from 60% to 80%, but it possesses the high effective thermal conductivity and large specific area. Fernández-Morales et al. [22] implemented experiments of heat transfer and pressure drop to determine the permeability and thermal conductivity of metal foam with 63.3-67.6% porosities, which indicates LPMF has the potential for application in the heat exchangers, electronic cooling systems, etc. The permeability of metal foam was obtained using the experimental method and "bottleneck" model by Furman et al. [23]. They found that theoretical model exhibited well with experimental data. Whereas relative to the HPMF, study for LPMF are still very few.

Many models were developed for predicting the thermal behavior of metal foam. Krishnan et al. [24] and Annapragada et al. [25] performed the numerical simulation of thermal transport for open-cell metal foam by using face-centered-cubic (FCC) model. Krishnan et al. Boomsma et al. [26] developed tetrakaidecahedron model which is employed to calculate the effective thermal conductivity of a saturated metal foam. [27] proposed the body-centered-cubic (BCC) according to the intricate geometry of metal foam and carried out the numerical simulation for effective thermal conductivity, pressure drop and local heat transfer coefficient. Whereas, these models are mainly used to numerically simulate thermophysical behavior of HPMF not for LPMF.

From the above literature, it can be found that HPMF has been subjected to intensive study. However, the study of LPMF is not enough. Particularly, the thermal behavior for LPMF filled with PCM is rarely studied at present, and the model used to predict the thermal performance of LPMF is also rarely proposed and investigated. Thus we combine the experimental and numerical approach to investigate the thermal behavior of PCM infiltrated in LPMF including the solid-liquid interface, temperature field, temperature history and effective thermal conductivity. The modified Kelvin model used for LPMF is developed and validated, which is of great significance for the study and design of TMS using composite PCM.

2. Description of experiment

2.1 Sample

In the present study, the low porosity aluminum foam is manufactured in University of Technology of Troyes by the infiltration casting method and selected as skeleton material. The infiltration casting method mainly consists of three steps: (1) the molten aluminum is poured into the mold which is filled with salt particle; (2) the liquid aluminum is infiltrated into the space of salt particle with the negative pressure condition; (3) the aluminum/salt composite is immersed in the water to remove the salt from the aluminum foam after the composite is cooled to room temperature. The rectangular aluminum foam samples of dimensions $60 \times 45 \times 25$ mm are prepared for experiments, as displayed in Fig. 1. Aluminum foam with 67% and 75% porosities and 10 PPI (pores per inch) pore density is used as experimental samples, in which the porosity is determined by the mass-volume direct

calculation $\varepsilon = (1 - \frac{m_f}{V_f \rho}) \times 100\%$ [17] and pore density is determined by the particle size of salt [28]. The paraffin R56 (provided by Merck Millipore) is used for experiment owing to the low melting point and high latent heat. The latent heat and transition temperature of paraffin are tested by differential scanning calorimeter (DSC) with the heating and cooling rate of 5 ℃/min. The DSC curve is displayed in Fig. 2. By analyzing the DSC curve, the melting range and latent heat of paraffin are determined. The thermophysical porosities of paraffin and aluminum are shown in Table 1.

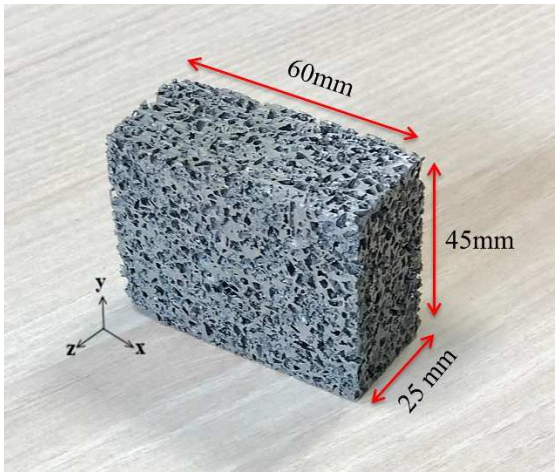

Fig. 1. Low porosity aluminum foam

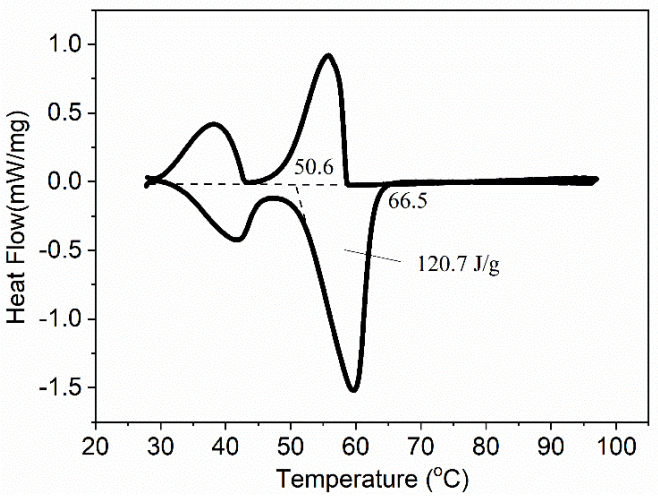

Fig. 2. DSC tested result of paraffin wax

Table 1
Thermophysical characteristics for paraffin and aluminum

Material	Property	Value
Paraffin	Specific heat ($J/(kg \cdot K)$)	2100
	Density (kg/m^3)	840
	Thermal conductivity ($W/(m \cdot K)$)	0.2
	Viscosity ($kg/(m \cdot s)$)	0.003
	Thermal expansion coefficient (K^{-1})	0.0004
	Latent heat (kJ/kg)	120.7
	Solidus temperature (K)	323.75
	Liquidus temperature (K)	339.65
Aluminum	Specific heat ($J/(kg \cdot K)$)	963
	Density (kg/m^3)	2680
	Thermal conductivity ($W/(m \cdot K)$)	160

2.2 Experimental apparatus

The schematic diagram of experimental setup used in this research is presented in Fig. 3. The setup is designed to obtain the temperature variation and capture phase transition evolvement. The rectangular aluminum foam ($60 \times 45 \times 25$ mm) is used for the experiment. A container is made by using transparent acrylic glasses and aluminum plate in order to hold the composite PCM and pure paraffin. The bottom of the container is the aluminum plate, which is attached with an electric heating film by using silicon paste to reduce the thermal contact resistance. Electric heating film used as heat source can provide the constant and uniform heat flux by controlling DC power. The top of the container is a thin aluminum sheet exposed to ambient air, which presents actual convective boundary condition in engineering applications. An observation window is designed by using optical glass as the front face of container to obtain infrared images, which is owing to that optical glass can availably transmit infrared of wavelength range of IR camera. The other faces consist of transparent acrylic glasses of thickness 2 mm. The front-back (z axis) faces of experimental setup are exposed to the environment, which conduces to the visualization of the melting evolution by using IR and HD camera. The polyurethane foam as insulation block is pasted on the left-right (x axis) faces of experimental setup to reduce the heat loss. Three T-type thermocouples are calibrated and fixed within composite at three different location (TC#1 (x=30 mm, y=10 mm), TC#2 (x= 30 mm, y=20 mm) and TC#3 (x=30 mm, y=30 mm)) along the symmetry axis of z direction to trace the temperature variation within samples during the

melting process. The data acquisition is used to automatically trace the temperature data from thermocouples and send the temperature data to the computer at regular time intervals. The snapshots of temperature field and solid-liquid melting evolution is extracted using the infrared camera and high definition camera. To investigate the thermal behavior enhancement of composite PCM, the rectangular pure paraffin sample of dimensions ($60\times45\times25$ mm) is also tested for comparison.

In this experiment, the uncertainty analysis is performed. The uncertainty is mainly attributed to the errors of power, thermocouple and filling volume. The uncertainty of power (ΔE) caused by DC power and heating film is 3.2%, which is provided by the manufacturer. The uncertainty of temperature (ΔT) associated with thermocouples is 0.1 ℃. The uncertainty of paraffin filling volume (ΔV) is 4.1%, which is caused by the void within composite PCM. It can be calculated by [29]:

$$\Delta V = (1-\frac{\Delta m}{\varepsilon V_f \rho_p})\times 100\% \tag{1}$$

Where, Δm is the mass difference between composite PCM and aluminum foam.

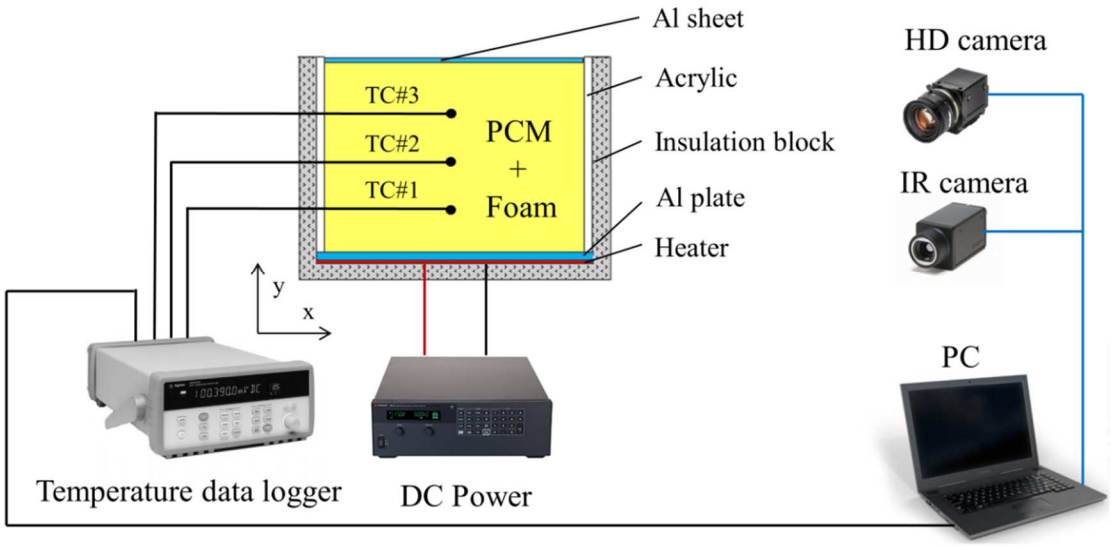

Fig. 3. Schematic diagram of experimental setup

3. Numerical investigation

3.1. Numerical model

The reconstruction of the intricate metal foam structure plays an important role in the pore-scale numerical simulation. There are several familiar models used to numerically simulate the thermal behavior of metal foam, such as tetrakaidecahedron, FCC and BCC etc. However, FCC and BCC models are not completely open-cell when porosity is below a certain limit, e.g., minimum porosity of experimental sample is 67%, and it is difficult to build by using FCC and BCC models. The modified Kelvin model was used to analyze the mechanical property of metal foam by Su et al [30]. It is proved that the modified Kelvin model can represent the property of metal foam. Also, the modified Kelvin model can remain

the open-cell structure as long as the porosity is greater than 50%. In present study, the modified Kelvin model is employed to simulate the thermal performance of LPAF. A tetrakaidecahedron is modeled to represent the salt particle. A unit cell of modified Kelvin model is created by cutting the tetrakaidecahedron from a solid cube, as presented in Fig. 4(a). To analyze the thermal behavior of metal foam using the pore-scale numerical method, the periodic distributed modified Kelvin cell is used to build the topology structure of aluminum foam. The dimensions of topology structure of aluminum foam are $60\times45\times25$ mm, which is equal to the dimensions of experimental sample, as shown in Fig. 4(b). The side length of solid cube is l and the distance between two opposite faces of the tetrakaidecahedron is a. The porosity of metal foam can be obtained by the following equation:

$$\varepsilon=\frac{9-\left(3-\frac{2l}{a}\right)^3}{16\left(\frac{l}{a}\right)^3}\times100\% \tag{2}$$

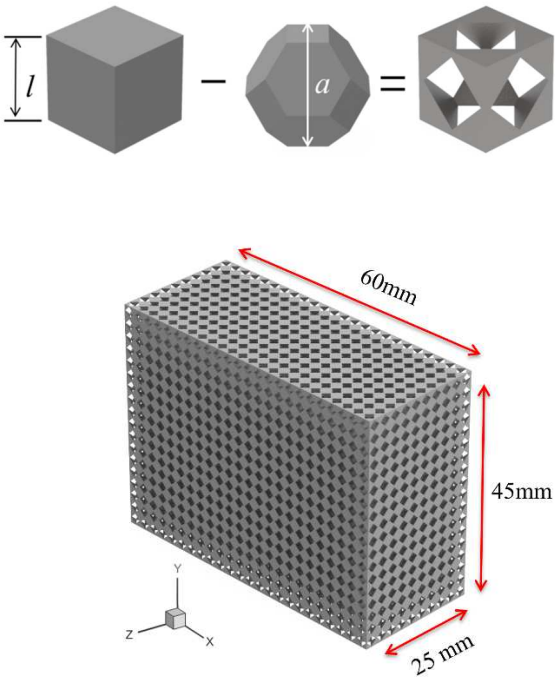

(a) (b)

Fig. 4. Numerical model of (a) a modified Kelvin unit cell (b) metal foam with periodic modified Kelvin cell

Numerical model is modeled according to the actual size of experimental samples to be used for simulation, which has a high requirement for computer performance and will consume too much computing time. Hence we conduct a study on the influence of number of cells in the x, y and z axis on thermal performance simulation. It is noted that the number of cells in the x axis has no influence on numerical results, which owes to the periodicity and symmetry of geometry and heat boundary condition. The number of cells in the y and z axis is decided according to the actual size of experimental samples, e.g., the length of b and d are 25mm and 45 mm respectively in this paper. Therefore, the computational zone consists of a

single slice composite PCM model in the left-right (x axis) direction to save the computing time, and paraffin (white) is filled into the cave of modified Kelvin cell to simulate the thermal behavior of composite PCM, as presented in Fig. 5. The boundary condition of numerical model is the same as the experimental design. The bottom face of model is imposed with constant heat flux. Due to the symmetry of model, the left-right faces are the symmetry boundary condition. A convective boundary condition is applied on the top and front-back (z axis) faces of model to simulation cooling situation by the air convection.

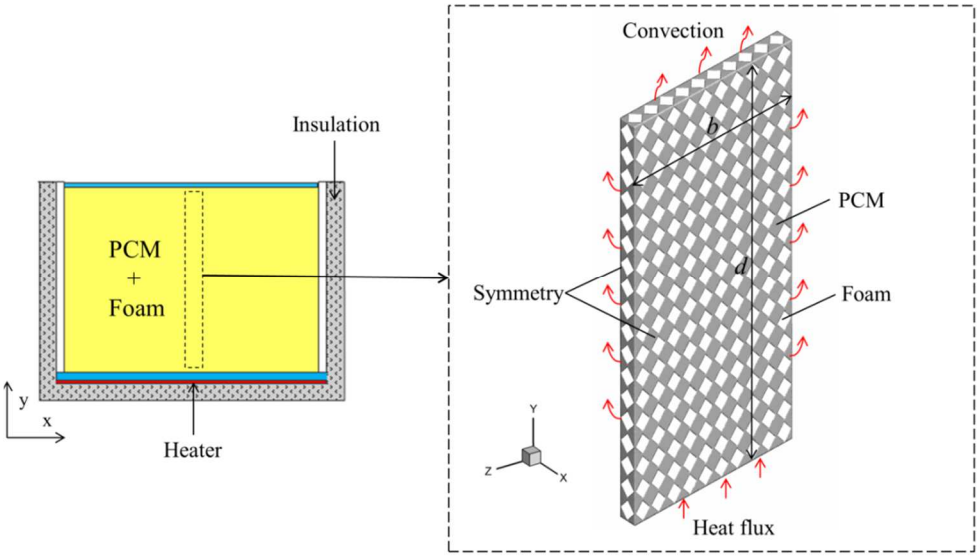

Fig. 5. Pore-scale numerical model of composite PCM with the boundary conditions

3.2. Numerical method

The pore-scale numerical model is established based on the following assumptions: (1) The thermophysical characteristics of PCM and metal foam are considered as homogeneous and constant during the phase change process; (2) The liquid phase paraffin is assumed to be incompressible and Newtonian; (3) The volume change of paraffin is ignored within the enclosed container and natural convection caused by buoyancy is simulated based on Boussinesq approximation.

Numerical model of composite PCM is enclosed, and there is no material exchange with the external. Hence, continuity equation is represented in Eq. (3):

$$\frac{\partial \rho_p}{\partial t} + \nabla \cdot (\rho_p \vec{u}) = 0 \tag{3}$$

Momentum equation:

$$\rho_p \frac{\partial \vec{u}}{\partial t} + \rho_p (\vec{u} \cdot \nabla)\vec{u} = \nabla \cdot \left[-p\vec{I} + \mu_p (\nabla \vec{u}) + \mu_p (\nabla \vec{u})^T \right] + \rho_p g \gamma (T - T_m) + S\vec{u} \tag{4}$$

Where, p is the pressure within composite PCM, $\vec{I}$ is a unit vector in x, y, and z directions.

The S in Eq. (4) is the parameter of damping force term for momentum equation, S can be defined as [31]:

$$S = \frac{(1-f_l)^2}{c+f_l^3} A_{\text{mush}} \tag{5}$$

Where, A_{mush} is the mushy zone constant, which can be employed to measure the amplitude of the damping and set to 1×10^5, and c is a smaller constant and set as 1×10^{-3} in this paper. f_l is the liquid fraction of PCM during the phase change process, as defined by:

$$f_l = \begin{cases} 0 & T < T_1 \\ (T-T_1)/(T_2-T_1) & T_1 < T < T_2 \\ 1 & T > T_2 \end{cases} \tag{6}$$

The heat transfer within composite PCM includes heat conduction, convective heat transfer and natural convection during the phase change process. Energy equation of heat transfer is given as follows:

The convective heat transfer for liquid PCM can be defined by:

$$\rho_p c_p \frac{\partial T_p}{\partial t} + \rho_p c_p \vec{u} \cdot \nabla T_p = \nabla\left(k_p \nabla T_p\right) - \rho_p L \frac{\partial f}{\partial t} \tag{7}$$

For heat transfer within metal foam, energy transport can be defined by:

$$\rho_f c_f \frac{\partial T_f}{\partial t} = \nabla \cdot \left(k_f \nabla T_f\right) \tag{8}$$

Conjugate heat transfer of the contact surface between PCM and metal foam can be written as follows:

$$T_p = T_f \tag{9}$$

$$k_p \frac{\partial T_p}{\partial n} = k_f \frac{\partial T_f}{\partial n} \tag{10}$$

3.3 Initial and boundary conditions

The initial temperature of composite PCM is the constant, which is the same as the ambient temperature ($T_0 = 20\,^{\circ}\text{C}$). It is written as follow:

$$T_p = T_f = T_0,\ 0 \leqslant x \leqslant l, 0 \leqslant y \leqslant d, 0 \leqslant z \leqslant b \tag{11}$$

The boundary conditions of composite PCM can be observed in Fig. 5. The bottom face of model is imposed with constant heat flux q. The top and front-back faces of model are the convective boundary condition. The other two faces are the symmetry boundary condition. The boundary condition used for governing equations can be defined as follows:

$$-k\frac{\partial T}{\partial x} = q,\ y = 0, 0 \leqslant x \leqslant l, 0 \leqslant z \leqslant b \text{ (bottom face)} \tag{12}$$

$$-k\frac{\partial T}{\partial x}=h_1(T_w-T_0),\ \ y=d,\ 0\ \leqslant\ x\ \leqslant l,\ 0\ \leqslant\ z\ \leqslant\ b \text{ (top face)} \tag{13}$$

$$-k\frac{\partial T}{\partial x}=h_2(T_w-T_0),\ \ z=0 \text{ or } d,\ 0\ \leqslant\ x\ \leqslant l,\ 0\ \leqslant\ y\ \leqslant\ d \text{ (front and back faces)} \tag{14}$$

$$-k\frac{\partial T}{\partial x}=0,\ \ x=0 \text{ or } l,\ 0\ \leqslant\ y\ \leqslant d,\ 0\ \leqslant\ z\ \leqslant\ b \text{ (left and right faces)} \tag{15}$$

Where, T_w is the face temperature of composite PCM, h is the heat transfer coefficient of natural convection caused by the temperature difference between the face and ambient air, which can be estimated by the empirical correlations [32]:

$$h_1=\frac{0.62k_{\text{air}}}{D}\left(GrPr\right)^{1/5} \tag{16}$$

$$h_2=\frac{0.59k_{\text{air}}}{D}\left(GrPr\right)^{1/4} \tag{17}$$

3.4. Computation setup

CFD Fluent 18.0 package is employed in numerical calculation. PISO algorithm is selected to couple the velocity-pressure term. Governing equations of momentum and energy are discretized employing second order upwind schemes and pressure equation is discretized adopting PRESTO approach. The high-performance computer and parallel processing are used for the present model considering a large number of grids. The computational domain of composite PCM is divided by ICEM CFD 18.0. The tetrahedron element is employed to mesh the domain of metal foam and PCM. The tetrahedron unstructured grid is conducive to the division of intricate structure for composite PCM. The mesh independence analysis is implemented to verify the precision of numerical results under the same boundary conditions. Three different numbers of grids (coarse grid of 3126k cells, medium grid of 5243k cells and fine grid of 9266k cells) are tested. The numerical results indicate that the difference of three grids is within 1%. Considering the accuracy of simulation and reducing the computation time, 5243k grids are selected, which can ensure mesh independence.

4. Results and discussion

4.1 Experimental results

To investigate melting evolution, the infrared camera is used to record the temperature variation of PCM. The infrared images of pure paraffin are displayed in Fig. 6, in which white presents the liquid phase and red presents the solid-liquid interface. The bottom of pure paraffin is heated by the horizontal heat source with heat flux 3500 W/m^2. At the initial stages of melting t = 800 s, the temperature of pure paraffin near heat source is higher than other location, while the most zones of pure paraffin are close to room temperature 20 ℃. This phenomenon is because a large amount of heat concentrates on the bottom owing to the low thermal conductivity of pure paraffin. The solid-liquid interface is parallel to the heat source, which indicates that the heat conduction dominates heat transfer at the beginning of melting. As time progresses, the interface gradually thickens and appears wavy owing to the effect of natural convection. The hot liquid near heat source flows upward and impinges on the

interface owing to the action of buoyancy, which is conducive to the heat exchange between liquid paraffin and solid paraffin. Natural convection gradually dominates the melting evolvement of pure paraffin. It is noted that the upper middle domain of pure paraffin melts fastest as shown in Fig. 6(d). While the left and right boundary zones of pure paraffin melt slower and temperature is lower, which is due to the heat loss from transparent acrylic glasses. Heat conduction and natural convection have combined effects on the melting process.

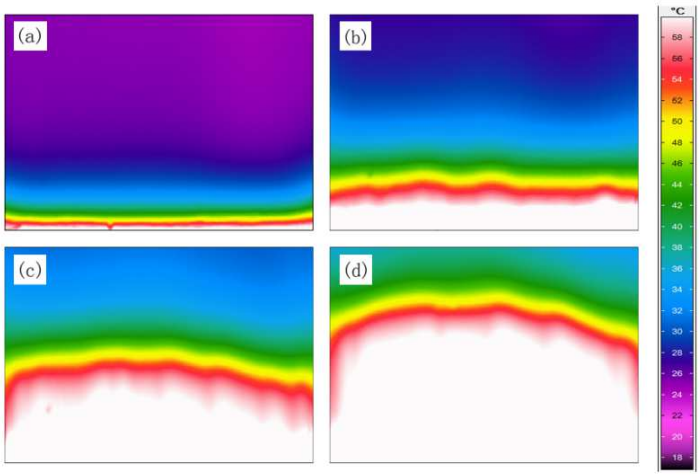

Fig. 6. Infrared images of pure paraffin at different time (a) t = 800 s (b) t = 1800 s (c) t = 2600 s (d) t = 3300 s

To distinctly display the melting evolvement of low porosity composite PCM, infrared images of composite PCM at difference time are presented in Fig. 7. Fig. 7(a) shows composite PCM which consists of the low porosity aluminum foam and pure paraffin. The temperature of composite PCM rapidly rises, and the average temperature is about 35℃ at t=500 s, which is owing to high thermal conductivity of LPMF. Also it is observed that there is temperature difference between aluminum skeleton and paraffin (observed by the black circle), which can demonstrate the existence of local thermal non-equilibrium phenomenon. As the melting progresses, the heat is quickly transferred between aluminum foam and paraffin, and the temperature difference between the bottom and top domain within composite PCM is about 20 ℃ at t = 750 s, which is smaller than 38 ℃ for pure paraffin at t = 800 s.

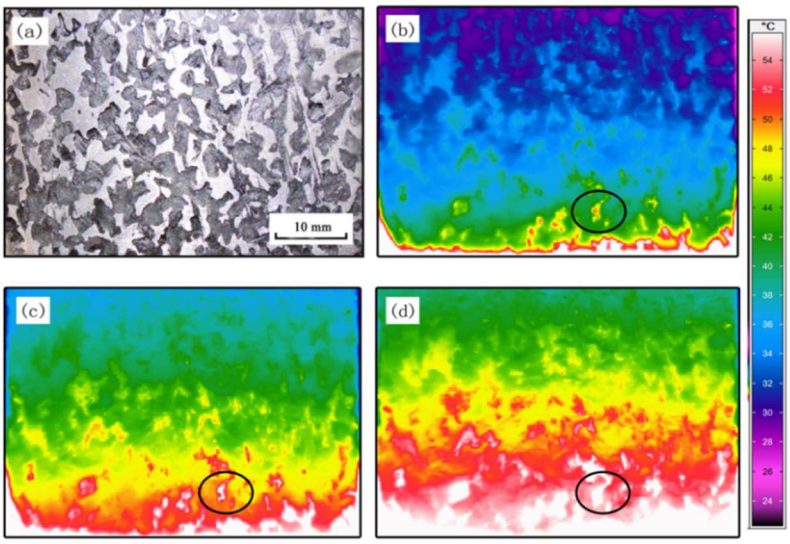

Fig. 7. (a) Experimental sample and infrared images at different time (b) t = 500 s (c) t = 750 s (d) t = 1000 s

To study the influences of porosity on thermal behavior, the snapshots of melting evolution for different porosities composite PCMs are obtained by directly capturing from the transparent acrylic glasses, as shown in Fig. 8. It is found that there is no obvious solid-liquid interface within composite PCM with 67% porosity. This is because effective thermal conductivity of composite PCM increases as the porosity decreases, which conduces to quick heat exchange between aluminum ligament and paraffin within the whole domain of composite PCM. Conversely, there is a relatively distinct interface within the composite with 75% porosity, which results from the combined action of natural convection and heat conduction. It is found from pictures that the melting time becomes longer as the increase of aluminum foam porosity, e.g., the paraffin within composite with 67% porosity has completely melted compared to composite with 75% porosity at 2460 s. By comparing with pure paraffin, the melting time of composite PCMs with 67% and 75% porosity is reduced by 45% and 36%, respectively.

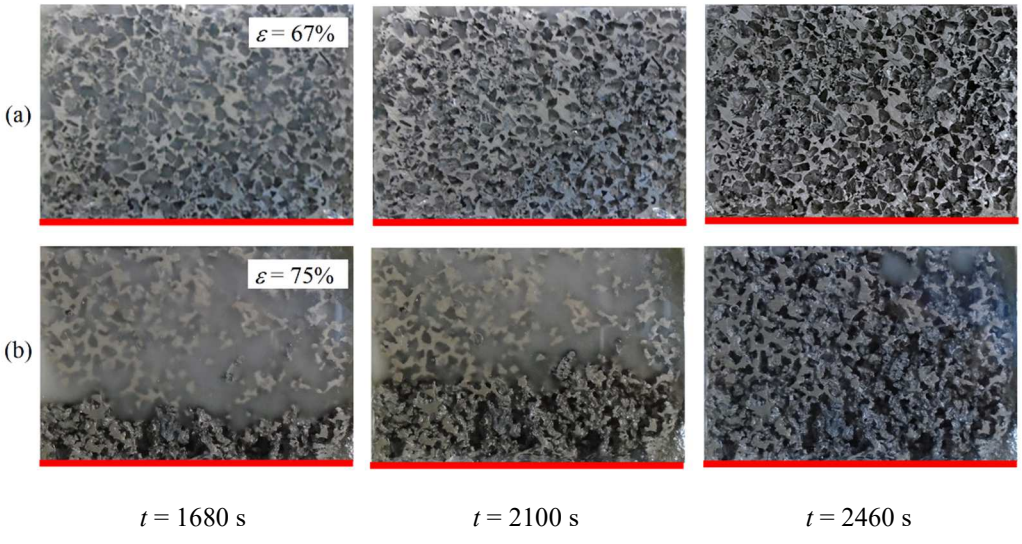

Fig. 8. Comparison of melting evolution for different porosities composite PCMs (a) ε = 67% (b) ε = 75%

The temperature difference between TC#1 and TC#3 during the melting process is presented in Fig. 9. The temperature difference curves of composite PCM for 67% and 75% porosities have a similar trend. The temperature difference firstly rises and then decreases. Moreover, it rises and then decreases again. The temperature difference of composite PCM gradually rises until it reaches the first maximum value, which is because a large amount of heat is accumulated at bottom domain in the vicinity of heat source in the initial stage of heating. Then the heat is transferred quickly from the bottom domain to top domain of composite PCM through the high conductivity metal skeleton, which results in that temperature difference reduces a few degrees and reaches a minimum value at the solid phase for paraffin. When the paraffin at the location TC#3 starts to melt, its temperature keeps a steady value. However, the temperature at the location TC#1 still continues to rise. Hence, the temperature difference between TC#1 and TC#3 reaches the second maximum value. Furthermore, it is observed that the temperature difference of 67% porosity composite is higher than that of 75% porosity composite in time ranging from 1690 s to 2000 s. This phenomenon is due to that paraffin within 67% porosity composite at TC# 3 location melts earlier, which results in that the increase rate of its temperature difference is larger than that of 75% porosity composite. Thus temperature difference of 67% porosity composite is higher. The temperature difference presents a slight decline after paraffin at the top domain melts. The maximum temperature difference of pure paraffin is 22.8 ℃ during the melting process, which is caused by low thermal conductivity of pure paraffin. The heat cannot be transferred quickly within pure paraffin, which results in the bigger temperature difference. Whereas the maximum temperature difference of composite PCM with 67% porosity is 3.8 ℃ and is reduced by 83.3% compared with pure paraffin. It can be confirmed that the temperature field within composite PCMs is the more uniform and thermal performance of PCM can be heightened by embedding low porosity aluminum foam.

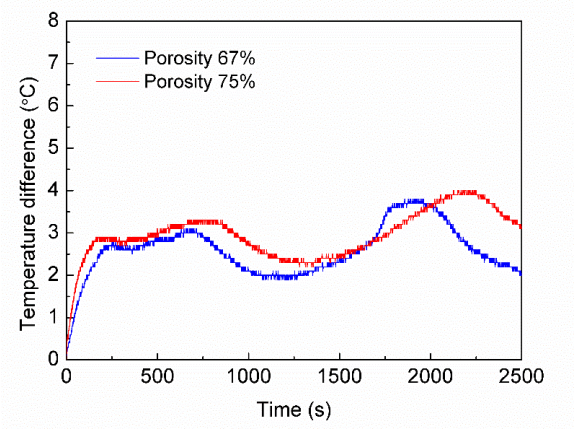

Fig. 9. Comparison of temperature difference between TC#1 and TC#3 during the melting process

4.2 Numerical results

The numerical results of modified Kelvin model are validated with the experiment data, in which aluminum foam with 75% porosity is impregnated with paraffin wax R56. The same constant heat flux 3500 W/m^2 and boundary conditions as the experiment are supplied to the numerical model. The temperature comparison of numerical results and experimental data at

three measurement points (TC#1, TC#2 and TC#3) is presented in Fig. 10. It is noted that the temperature variation of numerical simulation compares well with experimental data before the paraffin begins to melt. The numerical results are slightly larger than experimental data during the melting process. Also it is observed that the temperature rise rate of composite PCM is slower than before when the paraffin starts to melt, which is attributed to a large amount of energy stored in paraffin by the latent heat. It is demonstrated that modified Kelvin model can be applied to theoretically predict thermal characteristic of composite PCM with LPMF.

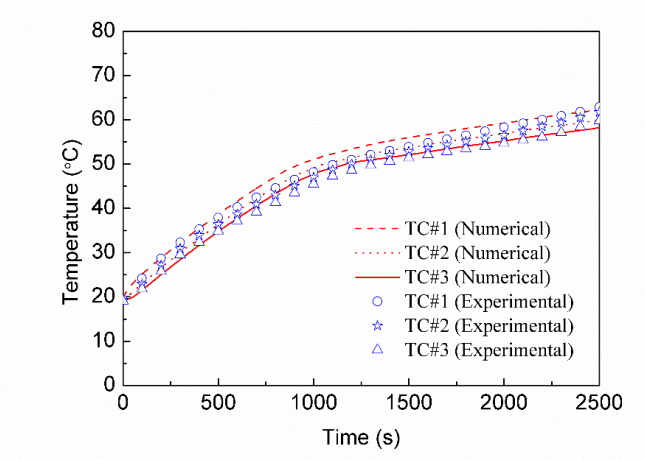

Fig. 10. Comparison of modified Kelvin model and experiment

The computational zone of numerical simulation is made up of a single slice composite PCM model in the x axis direction, as mentioned in section 3.1. To show the comparison of temperature distribution and infrared image, the model of composite PCM is cut into two part along the symmetry plane of x direction. The comparison of temperature distribution and infrared image at t = 1000 s is displayed in Fig. 11, in which the porosity of aluminum foam is 67%. It is found that the numerical result of temperature distribution is in good agreement with infrared image. This indicates that the modified Kelvin model can be used for pore-scale numerical simulation of composite PCM infiltrated in LPMF.

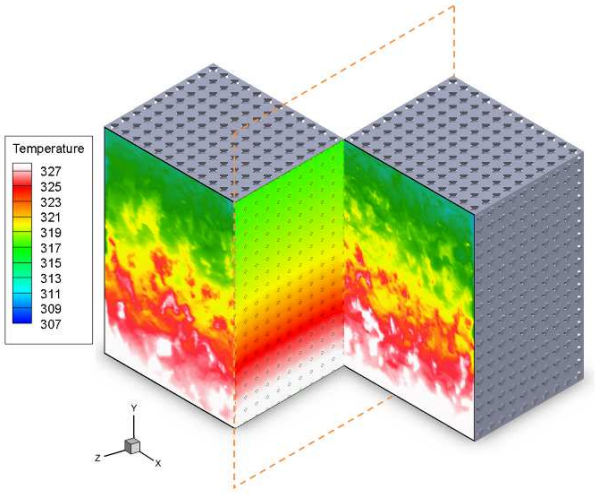

Fig. 11. Comparison of temperature distribution and infrared image

Accurate information on heat transfer and temperature distribution within composite PCM is critical for the design of TMS. The effective thermal conductivity is an important parameter and required in numerical models of thermal behavior for composite PCM. In this paper, the effective thermal conductivities of composites with different porosities are evaluated by the pore-scale numerical simulation in the steady state, based on the above successful demonstration of modified Kelvin model. The top and bottom walls are applied to the constant temperature 290 K and 310 K, respectively. All other walls are insulation, as displayed in Fig. 12(a). In present numerical simulation, two assumptions are recommended: (1) the heat transfer in composite is only heat conduction and one dimension; (2) the heat flux for any cross section is constant and equal along the direction of heat conduction (y direction). The effective thermal conductivity λ is calculated according to Fourier's equation:

$$Q = -A\lambda \frac{\mathrm{d}T}{\mathrm{d}x} \tag{18}$$

Upon convergence of the numerical solution, the heat flux over model under the constant temperature gradient can be extracted by integrating heat flux through top face or bottom face. As the heat flux and temperature gradient are obtained, the effective thermal conductivities of composite PCMs are evaluated based on Fourier's law. The comparison of effective thermal conductivity is displayed in Fig. 12(b). The thermal conductivity of paraffin is $0.2\,\mathrm{W/(m\cdot K)}$. Whereas, the effective thermal conductivities of composite PCMs for 67% and 75% porosities are $21.67\,\mathrm{W/(m\cdot K)}$ and $11.59\,\mathrm{W/(m\cdot K)}$, which are 108 and 58 times that of pure paraffin. It is proved that thermal conductivities can be obviously heightened by embedding LPMF in paraffin. It is noted that the numerical results of effective thermal conductivities compare well with the theoretical model developed by Boomsma et al, especially for the porosity 70%. It is also indicated that this theoretical model is proposed not only in the high porosity range but also in a certain low porosity range. There is a certain deviation between numerical results of effective thermal conductivities with the model prediction from Bhattacharya et al, which may be because the model prediction is recommended for use in the higher porosity range.

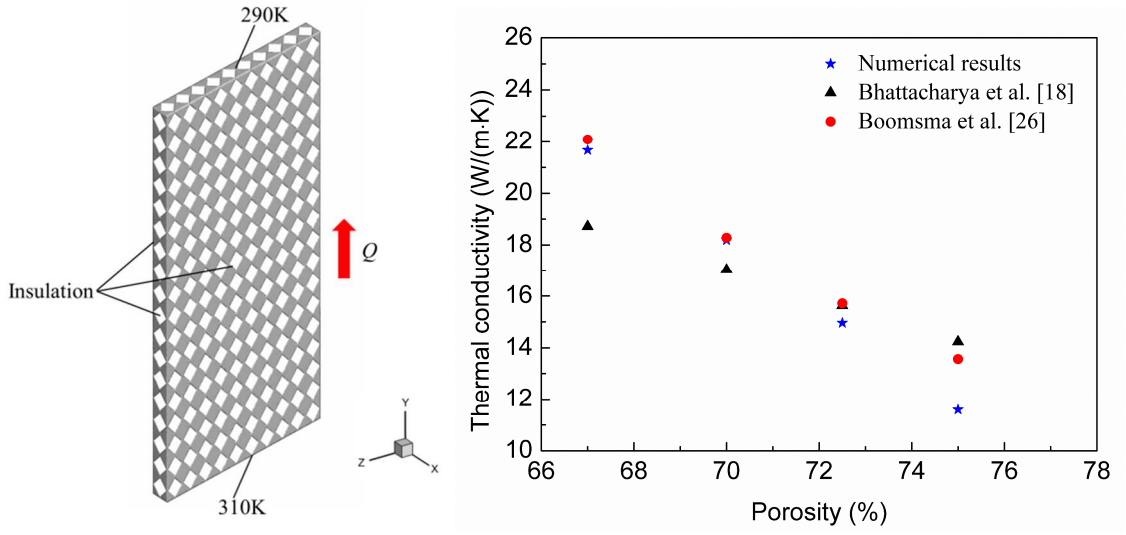

Fig. 12. (a) Numerical model in steady state (b) comparison of effective thermal conductivity of composite PCM

5. Conclusion

The thermal behavior of PCM with and without LPMF is experimentally and numerically investigated in this paper. The modified Kelvin model is developed to represent composite PCM and numerical results are compared to experimental data to verify the validity of model. Compared to that of pure paraffin, the melting time of composite PCM with 67% porosity can be reduced by 45%. The melting time of PCM infiltrated in LPMF can be significantly shortened, which is conducive to the improvement of efficiency for energy store in thermal management system. Besides, the temperature field is more uniform within composite PCM, e.g., the maximum temperature difference within composite PCM can be reduced by 83.3% compared with pure paraffin. It is found that the porosity has a distinct effect on the thermal performance. For instance, the melting time is extended as the increase of metal foam porosity and solid-liquid interface is not distinct for relatively lower porosity during the melting time. The numerical results of temperature histories and temperature distribution compare well with experimental data, which indicates modified Kelvin model can be used to predict the thermal performance of composite PCMs with LPMF. Also, it can be noted from results that effective thermal conductivities of PCM infiltrated in LPMF are drastically enhanced and numerical results are good in agreement with previous theoretical models. It is demonstrated form above results that the thermal performance of PCM is improved by embedding LPMF and modified Kelvin model is of great significance for study on the thermal behavior of composite PCM.

Acknowledgement

This research is supported by the Chinese Scholarship Council (CSC).

References

[1] Y. Tian, C.Y. Zhao, A review of solar collectors and thermal energy storage in solar thermal applications, Appl. Energy. 104 (2013) 538-553.

[2] A.M. Borreguero, A. Serrano, I. Garrido, J.F. Rodriguez, M. Carmona, Polymeric-SiO2-PCMs for improving the thermal properties of gypsum applied in energy efficient buildings, Energy Convers. Manage. 87 (2014) 138-144.

[3] S.F. Tie, C.W. Tan, A review of energy sources and energy management system in electric vehicles, Renewable and Sustainable Energy Reviews 20 (2013) 82-102.

[4] Z.H. Rao, S.F. Wang, A review of power battery thermal energy management, Renew Sust Energ Rev 15 (2011) 4554-4571.

[5] S. Shi, Y. Xie, M. Li, Y. Yuan, J. Yu, H. Wu, B. Liu, N. Liu, Non-steady experimental investigation on an integrated thermal management system for power battery with phase change materials, Energy Convers. Manage. 138 (2017) 84-96.

[6] W.X. Wu, X.Q. Yang, G.Q. Zhang, K. Chen, S.F. Wang, Experimental investigation on the thermal performance of heat pipe-assisted phase change material based battery thermal management system, Energy Convers. Manage. 138 (2017) 486-492.

[7] X. Yang, W. Wang, C. Yang, L. Jin, T.J. Lu, Solidification of fluid saturated in open-cell metallic foams with graded morphologies, Int. J. Heat Mass Transfer 98 (2016) 60-69.

[8] C. Ji, Z. Qin, Z. Low, S. Dubey, F.H. Choo, F. Duan, Non-uniform heat transfer suppression to enhance PCM melting by angled fins, Appl. Therm. Eng. 129 (2018) 269-279.
[9] A. Arshad, H.M. Ali, M. Ali, S. Manzoor, Thermal performance of phase change material (PCM) based pin-finned heat sinks for electronics devices: Effect of pin thickness and PCM volume fraction, Appl. Therm. Eng. 112 (2017) 143-155.
[10] C.Y. Zhao, G.H. Zhang, Review on microencapsulated phase change materials (MEPCMs): Fabrication, characterization and applications, Renew Sust Energ Rev 15 (2011) 3813-3832.
[11] S.A. Memon, H.Z. Cui, H. Zhang, F. Xing, Utilization of macro encapsulated phase change materials for the development of thermal energy storage and structural lightweight aggregate concrete, Appl. Energy. 139 (2015) 43-55.
[12] T. Li, J.-H. Lee, R. Wang, Y.T. Kang, Enhancement of heat transfer for thermal energy storage application using stearic acid nanocomposite with multi-walled carbon nanotubes, Energy 55 (2013) 752-761.
[13] T. Li, J.-H. Lee, R. Wang, Y.T. Kang, Heat transfer characteristics of phase change nanocomposite materials for thermal energy storage application, Int. J. Heat Mass Transfer 75 (2014) 1-11.
[14] Y. Yao, H. Wu, Z. Liu, Pore Scale Investigation of Heat Conduction of High Porosity Open-Cell Metal Foam/Paraffin Composite, J Heat Trans-T Asme 139 (2017).
[15] Q. Ren, Y.-L. He, K.-Z. Su, C.L. Chan, Investigation of the effect of metal foam characteristics on the PCM melting performance in a latent heat thermal energy storage unit by pore-scale lattice Boltzmann modeling, Numerical Heat Transfer Part a-Applications 72 (2017) 745-764.
[16] X. Hu, X. Gong, Pore-scale numerical simulation of the thermal performance for phase change material embedded in metal foam with cubic periodic cell structure, Appl. Therm. Eng. 151 (2019) 231-239.
[17] P. Liu, Introduction to porous materials, 2th ed., Beijing, Tsinghua University Press, 2012.
[18] A. Bhattacharya, V.V. Calmidi, R.L. Mahajan, Thermophysical properties of high porosity metal foams, Int. J. Heat Mass Transfer 45 (2002) 1017-1031.
[19] K. Lafdi, O. Mesalhy, S. Shaikh, Experimental study on the influence of foam porosity and pore size on the melting of phase change materials, J. Appl. Phys. 102 (2007).
[20] X. Yang, J. Yu, Z. Guo, L. Jin, Y.-L. He, Role of porous metal foam on the heat transfer enhancement for a thermal energy storage tube, Appl. Energy. 239 (2019) 142-156.
[21] X. Yang, P. Wei, X. Cui, L. Jin, Y.-L. He, Thermal response of annuli filled with metal foam for thermal energy storage: An experimental study, Appl. Energy. 250 (2019) 1457-1467.
[22] P. Fernández-Morales, C.A. Cano-Montoya, J.A. Pérez-Mesa, M.Á. Navacerrada, Thermal and permeability properties of metal aluminum foams for functional applications, Ingenieria y Universidad 21 (2016).
[23] E. Furman, A. Finkelstein, M. Cherny, Permeability of Aluminium Foams Produced by

Replication Casting, Metals 3 (2012) 49-57.
[24] S. Krishnan, S.V. Garimella, J.Y. Murthy, Simulation of Thermal Transport in Open-Cell Metal Foams: Effect of Periodic Unit-Cell Structure, J. Heat Transfer 130 (2008) 024503.
[25] S.R. Annapragada, J.Y. Murthy, S.V. Garimella, Permeability and thermal transport in compressed open-celled foams, Numer Heat Tr B-Fund 54 (2008) 1-22.
[26] K. Boomsma, D. Poulikakos, On the effective thermal conductivity of a three-dimensionally structured fluid-saturated metal foam, Int. J. Heat Mass Transfer 44 (2001) 827-836.
[27] S. Krishnan, J.Y. Murthy, S.V. Garimella, Direct Simulation of Transport in Open-Cell Metal Foam, J. Heat Transfer 128 (2006) 793.
[28] M.F. Ashby, A. Evans, N.A. Fleck, L.J. Gibson, J.W. Hutchinson, and H.N.G. Wadley, Metal foams: a design guide, Oxford, Butterworth-Heinemann, 2000.
[29] X. Xiao, P. Zhang, M. Li, Preparation and thermal characterization of paraffin/metal foam composite phase change material, Appl. Energy. 112 (2013) 1357-1366.
[30] Y.S. Su, Z.Q. Li, X.L. Gong, Q.B. Ouyang, Q. Guo, C.P. Guo, J. Zhang, D. Zhang, Structural modeling and mechanical behavior of Metal-Porous-Polymer-Composites (MPPCs) with different polymer volume fractions, Compos. Struct. 153 (2016) 673-681.
[31] ANSYS fluent software package: user's manual, 18.0, 2017.
[32] S. Yang, W. Tao, Heat transfer, 4th ed., Beijing, Higher Education Press, 2006.